Channel flow induced by wall injection of fluid and particles

Thierry Féraille[a] and Grégoire Casalis
ONERA, Aerodynamics and Energetics Modeling Department, 2, av. Edouard Belin, B.P. 4025, 31055 Toulouse cedex 4, France

(Received 30 January 2002; accepted 18 October 2002; published 7 January 2003)

The Taylor flow is the laminar single-phase flow induced by gas injection through porous walls, and is assumed to represent the flow inside solid propellant motors. Such a flow is intrinsically unstable, and the generated instabilities are probably responsible for the thrust oscillations observed in the aforesaid motors. However particles are embedded in the propellants usually used, and are released in the fluid by the lateral walls during the combustion, so that there are two heterogeneous phases in the flow. The purpose of this paper is to study the influence of these particles on stability by comparison with stability results from the single-phase studies, in a plane two-dimensional configuration. The particles are supposed to be chemically inert and of a uniform size. In order to carry out a linear stability study for this flow modified by the presence of particles, the mean particle velocity field is first determined, assuming that only the gas exerts forces on the particles. This field is sought in a self-similar form, which imposes a limit on the size of the particles. However, the particle mass concentration cannot be obtained in a self-similar form, but can only be described by a partial differential equation. The mean flow characteristics being determined, the spectrum of the discretized linear stability operator shows first that particle addition does not trigger any new ''dangerous'' modes compared with the single-phase flow case. It also shows that the most amplified mode in the case of the single-phase flow remains the most amplified mode in the case of the two-phase flow. Moreover, the addition of particles acts continuously upon stability results, behaving linearly with respect to the particle mass concentration when the latter is small. The linear correction to the monophasic mode, as well as the evolution of the modes with weak values of the particle mass concentration at the wall, are shown to be proportional to the ejection velocity of the particles. Then, the evolution of the eigenmodes from a given injection speed of the particles to another one is deduced by affinity, all other parameters being fixed. With a fixed Stokes number, stability results for a finite Reynolds number and results for the inviscid flow bring together when augmenting the particle mass concentration at the wall. Therefore, by knowing single-phase flow results and the evolution of stability characteristics of the two-phase flow in the inviscid case, it is easy to determine whether particle-laden Taylor flow is more or less stable than the monophasic Taylor flow for large particle mass concentration.
[DOI: 10.1063/1.1530158]

I. INTRODUCTION

Thrust of large solid propellant motors may exhibit oscillations whose frequency can be related to the longitudinal acoustic mode, though the flow inside the booster is predicted to be stable with conventional methods such as the acoustic balance. Varapaev and Yagodkin[1] and Casalis *et al.*[2] have shown that the flow induced by incompressible fluid injection through porous walls of a channel is intrinsically linearly unstable. The analytical laminar solution in a self-similar form of such a motion has been calculated by Taylor[3] in the case of an inviscid flow, the so-called ''Taylor flow.'' Viscosity is then easily introduced via the Reynolds number R, leading to a nonanalytical solution, but with the same similar form as the one of the Taylor flow. The solution obtained is assumed to be representative of the flow in the head of a booster (upstream part) in the case of a purely monophasic flow. The large curvature of the streamlines at the wall seems to be responsible for the instability of the flow,[4] so that this particular instability is called ''parietal instability.'' In cold gas experimental setup, reproducing Taylor flow, it has been observed that parietal instability leads to coherent structures able to excite acoustic modes.[5] This instability appears then to be one of the sources for inducing thrust oscillations. Currently, the problem is to couple instabilities and acoustic.[6–8]

Particles are introduced in the propellant because they increase its specific impulse on the one hand, and stabilize possible tangential pressure modes on the other hand. The influence of the particles on the stability of solid-propellant motors has been studied numerically by Dupays,[9] but only by considering the vortex shedding resulting from the shear layer initiated by the angular shape of the grain near the nozzle. The magnitude of the acoustic modes is also highly dependent on the presence of particles in the flow such as

[a]Author to whom correspondence should be addressed. Electronic mail: thierry.feraille@onecert.fr

recent computations performed by Lupoglazoff and Vuillot.[10] The effect of mass transfer between gas and particles on acoustic wave has also been studied by Daniel and Thévand.[11] They show that this effect is of great importance so that it can damp or increase the magnitude of an acoustic wave, even without wind. So the particles cannot have no effect on the stability of the wall injected flow, and this paper is the first attempt for modeling and quantifying the particle effect on such a motion. Moreover for this type of flow, their approach is purely numerical whereas the present one deals with the intrinsic instability.

Concerning the stability of particle-laden flows, plane Poiseuille flow with inert particles has been studied by Saffman,[12] especially by giving the asymptotic behavior of stability characteristics. Accurate computations have been carried out by Isakov and Rudnyak.[13] The most important result in these two papers is that the addition of particles into a flow does not only stabilize it, as one can reasonably imagine, but can also destabilize it by increasing the mass density of the gas and thus the Reynolds number R. Another conclusion[12] is that the stabilizing effect reaches a maximum for given values of mass concentration and relaxation time. Computations by Isakov *et al.* corroborate these results but also indicate that, under certain conditions, the neutral curve of stability re-loops, creating an ''instability island'' in the plane (R,α). (Isakov uses a temporal stability theory in which α is a real wave number.) These studies show the complex influence of particles on stability characteristics, but only for the plane Poiseuille flow.

One goal of the present paper is to determine if the addition of particles in Taylor flow would also lead to a complex behavior, as in the case of Poiseuille flow. The main interest is to know how particle addition modifies monophasic stability results and whether some particle sizes have to be favored or avoided regarding their influence on stability characteristics. The general assumptions are first that particles are inert and have the same temperature as the gas, therefore there is no thermal effect that can induce compressibility. Moreover we assume that there is only one kind of spherical particles.

In the case of particle-laden Taylor flow, an Eulerian approach of the two-phase flow is retained, as has been done in the above-mentioned studies, accordingly both gas flow and particle motion are represented by a velocity field and a mass density field; this is described in Secs. II and III of the paper. Because of the particle inertia and the nonparallel nature of Taylor flow, gas velocity, and particle velocity fields cannot be identical, thus a new solution for the flow with particles induced by gas injection through porous walls is sought in Sec. IV. A one-way coupling computation is assumed to be efficient, which limits particle mass concentration ρ_p (defined in the following) and Stokes number S for comparisons with practical configurations. After the determination of the so-called ''mean flow,'' a linear stability study is carried out in Sec. V, leading to an eigenvalue problem. The results described in Sec. V are the following ones. By using a standard small perturbation technique applied to the injected particle mass concentration, it is first proved that the stability properties vary continuously from the single-phase Taylor flow stability results. In addition, spectrum analysis seems to prove that particles do not add any amplified modes in comparison with the monophasic Taylor flow. The most amplified mode is finally considered for the parametric study concluding this stability analysis. The complex influence of dust in flows is still observable as is the case for the particle-laden Poiseuille flow.

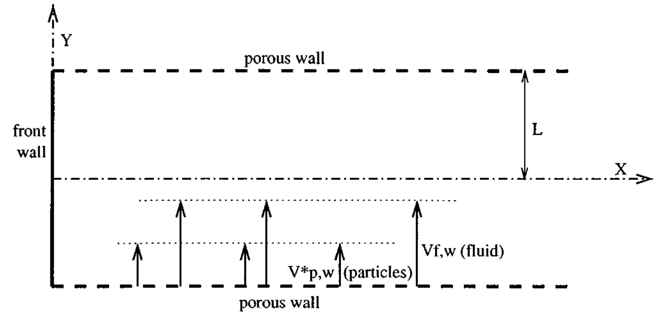

FIG. 1. Geometric configuration scheme.

II. GEOMETRY

The study is based on a two-dimensional plane flow induced by fluid and particle injection from lateral porous walls of a $2L$ height channel. The gas speed at the propellant boundary is $V_{f,w}$, while the speed of a solid particle released from the wall is $V^*_{p,w}$. The x axis corresponds to the streamwise axis and is the symmetry line of the channel, the y axis is orthogonal, as shown in Fig. 1. The channel is closed at the front wall $x=0$, defining a semi-infinite channel for $x \geqslant 0$. The reference length is half the channel height L and the reference speed is $V_{f,w}$ for both fluid and particle motions. Fluid streamlines and the velocity gas flow field for the Taylor flow solution (see Casalis *et al.*[2] and Sec. IV A) are presented in Fig. 2.

III. TWO-PHASE FLOWS

We consider an incompressible gas of density ρ_f and dynamic viscosity μ with the velocity field $\mathbf{V}_f = V_{f_i}(X_i, T)$, where T represents time. Using the Eulerian approach, we define a velocity field $\mathbf{V}_p = V_{p,i}(X_i, T)$ and a number density field $N(X_i, T)$ for the solid dispersed phase, N represents the number of particles per unit volume. In order to simplify the problem, we suppose uniform spherical rigid particles of radius a and of material density ρ_p^o. We also assume $a \ll L$, so that the resulting Reynolds number $R_p = \rho_f a \|\mathbf{V}_p - \mathbf{V}_f\| / \mu$ is

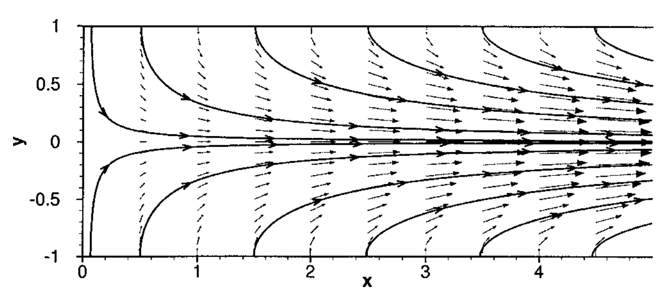

FIG. 2. Fluid streamlines and velocity profiles.

small and the problem can be treated with the Stokes approximation. Moreover, the bulk concentration $\rho_p(\rho_f/\rho_p^o)$ is assumed to be small (ρ_p is the particle mass concentration, as will be defined later), so that the only force applied on a particle is the viscous Stokes drag $\mathbf{F}_S = F_{Si} = 6\pi a\mu(V_{f,i} - V_{p,i})$. The terms corresponding to the effects of the undisturbed flow pressure gradient, the added mass, the buoyancy, and the Basset history term are neglected. Due to these assumptions, the mass conservation equation for the particles and the particle motion equations are

$$\frac{\partial N}{\partial T} + \frac{\partial N V_{p,i}}{\partial X_i} = 0, \tag{1}$$

$$m_p N\left(\frac{\partial V_{p,i}}{\partial T} + V_{p,j}\frac{\partial V_{p,i}}{\partial X_j}\right) = 6\pi a\mu N(V_{f,i} - V_{p,i}), \quad i=1,2,3, \tag{2}$$

with $m_p = \frac{4}{3}\pi a^3 \rho_p^o$ the mass of a particle. So $m_p N(X_i,t)$ is the mass of particles per unit volume.

In order to satisfy the momentum conservation for the system {gas+particles}, the Stokes drag term, written on the right-hand side of (2), must be subtracted in the momentum equation written for the gas:

$$\rho_f\left(\frac{\partial V_{f,i}}{\partial T} + V_{f,j}\frac{\partial V_{f,i}}{\partial X_j}\right) = -\frac{\partial P}{\partial X_i} + \mu\frac{\partial^2 V_{f,i}}{\partial X_j \partial X_j} - 6\pi a\mu N \times (V_{f,i} - V_{p,i}), \quad i=1,2,3. \tag{3}$$

The incompressibility of the gas yields

$$\frac{\partial V_{f,i}}{\partial X_i} = 0. \tag{4}$$

Using the length scale L and the reference velocity $V_{f,w}$, we easily obtain the nondimensional quantities:

$$v_{f,i} = \frac{V_{f,i}}{V_{f,w}}, \quad t = \frac{V_{f,w}}{L}T,$$
$$v_{p,i} = \frac{V_{p,i}}{V_{f,w}}, \quad p = \frac{P}{\rho_f V_{f,w}^2}, \tag{5}$$
$$x_i = \frac{X_i}{L}, \quad \rho_p = \frac{m_p N}{\rho_f}.$$

In the following x_1 and x_2 represent x and y, respectively. These variables lead to the following nondimensional equations for the gas and particles:

$$\frac{\partial v_{f,i}}{\partial t} + v_{f,j}\frac{\partial v_{f,i}}{\partial x_j} = -\frac{\partial p}{\partial x_i} + \frac{1}{R}\frac{\partial^2 v_{f,i}}{\partial x_j \partial x_j} + \frac{\rho_p}{S}(v_{p,i} - v_{f,i}), \quad i=1,2,3, \tag{6}$$

$$\frac{\partial v_{f,i}}{\partial x_i} = 0, \tag{7}$$

$$\frac{\partial \rho_p}{\partial t} + \frac{\partial \rho_p v_{p,i}}{\partial x_i} = 0, \tag{8}$$

$$\frac{\partial v_{p,i}}{\partial t} + v_{p,j}\frac{\partial v_{p,i}}{\partial x_j} = \frac{1}{S}(v_{f,i} - v_{p,i}), \quad i=1,2,3. \tag{9}$$

The expressions of the Reynolds number R and Stokes number S are

$$R = \frac{\rho_f V_{f,w} L}{\mu}, \quad S = \frac{2}{9}\left(\frac{a}{L}\right)^2 \frac{\rho_p^0 V_{f,w} L}{\mu}. \tag{10}$$

Obviously, the smaller the radius a and the material density ρ_p^o of the particle are, the smaller the Stokes number is. Such an observation means that the smaller the Stokes number is, the smaller the inertia of the particle is, and the better the particle reactivity is to a fluid perturbation.

IV. MEAN FLOW

We look for a steady solution in the set $\{(x,y) \in [0,\infty[\times[-1,1]\}$. The line $y=0$ is also the symmetry line for the flow. Since the solid phase is very diluted, one-way coupling computations would be efficient. In fact, one-way coupling computations are efficient, with the point of view of stability for quite low Stokes number and low particle mass ratio (the latter being the ratio of the mass of particles released on the total mass of gas and particles injected in the channel), see Féraille *et al.*[14] In the aforementioned paper, it is shown that the admissible particle mass ratio depends on the Stokes number of the particles. It is about 20% for Stokes number of about 10^{-3} and more than 5% for Stokes number of about 0.1. Moreover, the Stokes number is assumed to be small, particles thus have no effect on gas; the Stokes drag term is neglected in the equations for the fluid motion (6): the gas velocity field is identical to the one issued in the monophasic study (this assumption only concerns the mean flow, see Sec. V).

As in the single-phase studies, solutions for the fluid stream function $\psi(x,y)$ and particle transverse and longitudinal velocities, V_p and U_p, are sought in self-similar forms:

$$\psi(x,y) = xF(y),$$
$$v_{p,1}(x_i) = U_p(x,y) = xG(y), \tag{11}$$
$$v_{p,2}(x_i) = V_p(y) = J(y).$$

The mass concentration ρ_p will be computed both in self-similar form and in its most general form:

$$\text{self-similar form} \quad \rho_p = H(y),$$
$$\text{general form} \quad \rho_p = \rho_p(x,y). \tag{12}$$

From these assumptions, an ordered system of equations is obtained. After the already known gas mean flow, the particles' transverse velocity V_p may first be determined, then the longitudinal velocity of the particles U_p, and finally the particle mass concentration as described in the following.

A. Fluid velocity field

Introducing the stream function $\psi(x,y) = xF(y)$ in the simplified equation (6), the differential equation for F is[15]

$$F'F''-FF'''=\frac{1}{R}F^{(IV)}, \tag{13}$$

associated with the following boundary conditions:

$$F(-1)=-1, \quad F'(-1)=0, \quad F(1)=1, \quad F'(1)=0. \tag{14}$$

In the case of an inviscid flow, Taylor[3] found an analytical solution:

$$\forall x \geqslant 0, \ \forall y \in [-1,1], \quad \psi(x,y)=x \sin\left(\frac{\pi}{2}y\right). \tag{15}$$

Alternatively, the solution is computed from (13) and (14). For Reynolds number larger than 1000, it appears that the analytical solution is very close to the computed one (see Ref. 2). In both cases, the only point where transverse fluid velocity is equal to zero is the line $y=0$.

B. Transverse velocity V_p

The above-given assumptions induce some restrictions on the calculations of the solution as explained in the following. The equation for V_p is

$$JJ'+\frac{F+J}{S}=0. \tag{16}$$

The problem would be still incomplete without the following boundary condition:

$$J(-1)=\frac{V^*_{p,w}}{V_{f,w}}=V_{p,w}, \quad V_{p,w}>0, \tag{17}$$

where $V_{p,w}$ is the nondimensional particle velocity at the lower propellant surface. A similar condition can be written for particles from the upper propellant surface: $J(1)=-V_{p,w}$. The gas transverse velocity is zero at the symmetry line, it may be expected that there exists a position y_1 for which $J(y_1)=0$. In this case, at the point $y=y_1$, the differential equation (16) is not Lipschitzian and the problem is not defined correctly. [A differential equation in the form $z'=\phi(y,z)$ is said to be Lipschitzian if the function ϕ is K Lipschitzian with respect to the second variable z, i.e., $\exists K>0/\forall(y,z_1,z_2)\ |\phi(y,z_1)-\phi(y,z_1)|\leqslant K|z_1-z_2|$. If ϕ is continuous with respect to the two variables y and z and is K Lipschitzian with respect to z, the Cauchy–Lipschitz theorem indicates that the differential equation admits only one solution with boundary conditions of Cauchy type. In the case of Eq. (16), the function $\phi=\phi(y,J)$ is clearly not Lipschitzian.] For (16) and (17), the transverse position y_1 can only be positive: the particle carried by the fluid and by its own inertia cannot stop before the fluid stops at $y=0$, it may only cross the line $y=0$. Then, two kinds of solutions, leading to two different behaviors, will be distinguished:

(1) $y_1=0$, the particle transverse velocity value is zero on the symmetry line.
(2) $y_1>0$, the particle transverse velocity value is nonzero on the symmetry line.

By considering the first hypothesis ($y_1=0$), in order to know how the solution J evolves near 0, order 1 limited expansions for F and J are written as

$$F(y)=F'(0)y+o(y), \quad J(y)=J_1y+o(y).$$

Introducing these expansions in Eq. (16) leads to the following quadratic equation:

$$J_1^2+\frac{1}{S}J_1+\frac{1}{S}F'(0)=0.$$

This equation admits two real solutions only if the following condition is fulfilled:

$$S\leqslant\frac{1}{4F'(0)}. \tag{18}$$

To observe this condition, the only possible solution is

$$J_1=\frac{-1+\sqrt{1-4SF'(0)}}{2S}. \tag{19}$$

As expected, $\lim_{S\to 0}J_1=-F'(0)$, which is the clean gas transverse velocity. Then, the time T a particle needs to travel from the propellant surface ($y=-1$) to the position y_1 is determined by

$$\int_0^T dt=\int_{-1}^{y_1=0}\frac{dy}{V_p(y)}.$$

$1/V_p$ behaves as $1/y$ near 0, so that the above-given expression indicates that the particles never reach the line $y=0$.

On the other hand, if condition (18) is not observed, the two solutions for J_1 would be complex, therefore unphysical. The relation $V_p=0$ cannot be used at $y_1=0$, but only at $y_1>0$. In that case, the behavior of the solution near the position y_1 is found in the form

$$J(y)=\sqrt{\frac{2F(y_1)}{S}}(y_1-y)^{1/2}+o(y_1-y)^{1/2}.$$

Then the new position $y_1>0$ can be reached in a finite time, whereas $y_1=0$ has previously be found to be an asymptotic position. In addition with the circular curvature of the streamline imposed by the $\sqrt{y_1-y}$ behavior at y_1, particles would oscillate around $y=0$. In this case, the solution in self-similar form $V_p(x,y)=J(y)$ is no longer acceptable. Thus the present study is limited to flows satisfying condition (18).

Taking into account this conclusion, the analysis may be limited to a half-domain. We choose the lower domain $\{(x,y)\in[0,\infty[\times[-1,0]\}$.

C. Longitudinal velocity U_p

The projection of the particle momentum equation on the x axis is

$$JG'=\frac{F'-G}{S}-G^2. \tag{20}$$

The associated boundary condition is

$$G(-1)=0. \tag{21}$$

This condition, in addition to (17), means that the particle is orthogonally released from the plane surface of the propellant. With condition (18), the longitudinal component of the particles' velocity reaches a maximum at the line $y=0$ for each x coordinate. With the same treatment near the symmetry line as the one for the determination of J, the maximum of G is located at $y=0$ and has the following value:

$$G(0)=G_0=\frac{-1+\sqrt{1+4SF'(0)}}{2S}. \tag{22}$$

As $G_0 \leqslant F'(0)$, the maximum particle velocity is smaller than the maximum gas velocity, as expected.

D. Particle mass concentration ρ_p

The functions J and G being determined, particle mass concentration inside the channel can be now calculated.

As has been done for U_p and V_p, the first idea is to seek ρ_p in a self-similar solution $H(y)$. The first requirement is to impose a uniform boundary condition at the wall:

$$H(-1)=\rho_{p,w}, \tag{23}$$

where $\rho_{p,w}$ is a constant value. Then Eq. (8) reduces to

$$HG+JH'+J'H=0. \tag{24}$$

However, as will be explained in the following section, this self-similar solution is not bounded at $y=0$. In order to avoid this nonphysical behavior, ρ_p must be fixed to 0 at the front wall (there is no particle injection at the front wall). In that case, the boundary condition must be dependent on the x coordinate and becomes

$$\forall x \in [0,\infty[, \rho_p(x,-1)=\tilde{\rho}_{p,w}(x), \tag{25}$$

with $\tilde{\rho}_{p,w}=0$ at $x=0$ and $\lim_{x\to\infty}\tilde{\rho}_{p,w}(x)=\rho_{p,w}$. A self-similar solution is no longer possible, Eq. (8) is now a partial differential equation:

$$\rho_p G+xG\frac{\partial\rho_p}{\partial x}+J\frac{\partial\rho_p}{\partial y}+J'\rho_p=0. \tag{26}$$

In a practical way, the $\tilde{\rho}_{p,w}$ function is the concatenation of a constant value function (equal to $\rho_{p,w}$) for $x>x_0$ and of an increasing function from 0 for $x=0$ to $\rho_{p,w}$ for $x=x_0$. In Fig. 3, the two kinds of solution ρ_p and H are plotted for $V_{p,w}=0.1$, $x_0=1$ at the abscissas $x=2,4,6,8,10$. As mentioned previously, H exhibits a diverging behavior close to the symmetry line. Apart from this region, ρ_p and H are nearly identical. Moreover, it must be pointed out that particle mass concentration ρ_p has a nearly constant value on the major part of the channel height. An estimation of this plateau is noted P_ρ (see Fig. 3).

1. *H behavior*

In order to explain the divergence of the solution H near $y=0$, let us define a point of y-coordinate l located in the vicinity of the symmetry line. Then Eq. (24) can be expanded for $|y-l|\ll 1$ in

$$J_1 yH'+(G_0+J_1)H+o(y-l)=0, \tag{27}$$

using J_1 and G_0 from (19) and (22). The solution of this equation is

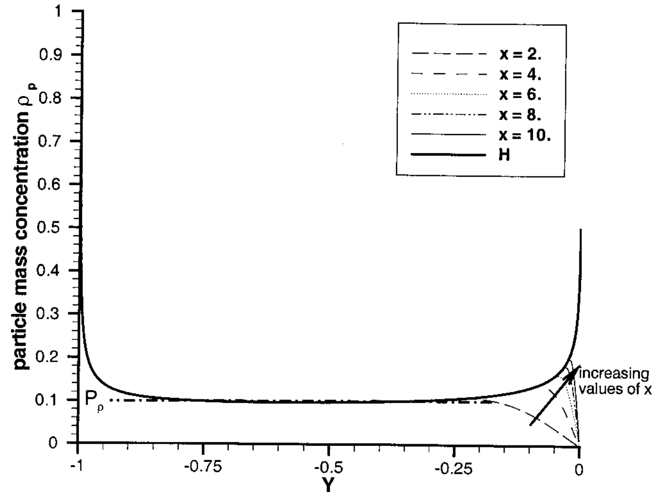

FIG. 3. Comparison of the self-similar form solution H and the PDE solution ρ_p of the particle mass concentration at $x=2, 4, 6, 8, 10$ with $x_0=1$. $R=10^3$, $S=10^{-1}$, $V_{p,w}=0.1$, and $\rho_{p,w}=1$. Apparition of a plateau P_ρ between $y=-0.9$ and $y=-0.25$, $P_\rho \simeq V_{p,w}\rho_{p,w}=0.1$.

$$H(y)=H(l)\left(\frac{y}{l}\right)^{-(1+G_0/J_1)}.$$

Due to expressions (19) and (22), the coefficient $(1+G_0/J_1)$ is always positive for flows obeying condition (18), so that the solution is divergent near the symmetry line. That is the reason why we rather work with the complete partial differential equation problem $\{(26)+(25)\}$, which has a zero value at the symmetry line.

2. *ρ_p behavior*

Compared with the fluid flow, the divergence of the particle velocity field $(\partial v_{pi}/\partial x_i)$ has a nonzero value because ρ_p is not constant. More precisely $(\partial v_{pi}/\partial x_i)(0)=G_0+J_1<0$, so that there is a contraction of the volume near the line $y=0$, and then the particle mass concentration increases close to the symmetry line as the function H does. Thus it appears that H may be a good candidate for an asymptotic approximation of ρ_p for $x\gg 1$. Actually, in order to prove this assertion, let us consider the function $\mathcal{R}(\chi,y)=\rho_p(x,y)$, with $\chi=1/x$. For $y\in[-1,\eta]$ with $\eta<0$ and for $x\gg 1$, the function $\mathcal{R}$ can be sought in the form

$$\mathcal{R}(\chi,y)=\mathcal{R}_0(y)+O(\chi).$$

Equation (26) gives the following equation at order 0 for χ, except close to $y=0$ where $\mathcal{R}$ depends strongly on the x coordinate:

$$J\mathcal{R}_0'+(G+J')\mathcal{R}_0=0, \tag{28}$$

which is identical to Eq. (24). Furthermore, we assume that $\tilde{\rho}_{p,w}\to\rho_{p,w}$ as $x\to\infty$ so that the boundary condition associated with $\mathcal{R}_0$ is

$$\mathcal{R}_0(-1)=\rho_{p,w}.$$

Finally, the problem for $\mathcal{R}_0$ is identical to the problem for H, so $\mathcal{R}_0\equiv H$. The agreement between both solutions is shown in Fig. 3.

Even if the evolutions of ρ_p and H are the same on a large extent of the y coordinate, we shall work with the complete problem $\{(26)+(25)\}$ to avoid any problem with the stability study.

V. STABILITY STUDY

Now that the mean flow is determined, a linear stability theory can be applied. Although we are aware that our approach is not consistent,[16] we consider perturbation q' in the normal mode form

$$q'(x,y,t)=\hat{q}(y)\exp i(\alpha x-\omega t),$$

as is usually assumed for a strictly parallel mean flow. Mathematically, the factorization of the perturbation into the normal mode form is not valid in the case of the Taylor flow, because the basic flow depends on the streamwise coordinate x. As a consequence, stability results depend on the formulation of the problem.[4] Despite this approximation, studies on the monophasic flow have shown good agreement with results obtained with more consistent approaches and with experiments.[5]

Linearizing Eqs. (6)–(9) (in which the action of the particles toward the flow is no longer neglected) and introducing the expression of the above-determined mean flow lead to the following system:

$$i\alpha\hat{u}_f+\frac{d\hat{v}_f}{dy}=0, \tag{29}$$

$$-i\omega\hat{\rho}_p+i\alpha\hat{\rho}_p xG+G\hat{\rho}_p+J\frac{d\hat{\rho}_p}{dy}+J'\hat{\rho}_p+\frac{\partial\overline{\rho_p}}{\partial x}\hat{u}_p+i\alpha\overline{\rho_p}\hat{u}_p$$
$$+\frac{\partial\overline{\rho_p}}{\partial y}\hat{v}_p+\overline{\rho_p}\frac{d\hat{v}_p}{dy}=0, \tag{30}$$

$$-i\omega\hat{u}_f+\hat{u}_fF'+\hat{v}_fxF''+i\alpha x\hat{u}_fF'-F\frac{d\hat{u}_f}{dy}$$
$$=-i\alpha\hat{p}+\frac{1}{R}\left(\frac{d^2\hat{u}_f}{dy^2}-\alpha^2\hat{u}_f\right)$$
$$+\frac{\hat{\rho}_p}{S}x(G-F')+\frac{\overline{\rho_p}}{S}(\hat{u}_p-\hat{u}_f),$$
$$-i\omega\hat{v}_f-\hat{v}_fF'+i\alpha x\hat{v}_fF'-F\frac{d\hat{v}_f}{dy} \tag{31}$$
$$=-\frac{d\hat{p}}{dy}+\frac{1}{R}\left(\frac{d^2\hat{v}_f}{dy^2}-\alpha^2\hat{v}_f\right)+\frac{\hat{\rho}_p}{S}(J+F)+\frac{\overline{\rho_p}}{S}(\hat{v}_p-\hat{v}_f),$$

$$-i\omega\hat{u}_p+\hat{u}_pG+i\alpha\hat{u}_pxG+\hat{v}_pxG'+J\frac{d\hat{u}_p}{dy}=\frac{1}{S}(\hat{u}_f-\hat{u}_p),$$
$$-i\omega\hat{v}_p+i\alpha\hat{v}_pxG+\hat{v}_pJ'+J\frac{d\hat{v}_p}{dy}=\frac{1}{S}(\hat{v}_f-\hat{v}_p). \tag{32}$$

Such a system can be written as a first-order system of seven ordinary differential equations:

$$\mathcal{L}.\mathcal{Z}=\left(\frac{d\cdot}{dy}-D\cdot\right).\mathcal{Z}=0,$$

with the unknown column vector:

$$\mathcal{Z}=\left(\hat{u}_f,\frac{d\hat{u}_f}{dy},\hat{v}_f,\hat{p},\hat{u}_p,\hat{v}_p,\hat{\rho}_p\right)^T.$$

The 7×7 matrix D is given in Appendix A.

In system (29)–(32), equations for particles are non-Lipschitzian on the axis $y=0$—because $V_p(0)=J(0)=0$, as seen earlier. So Eqs. (30) and (32) cannot be integrated between the two physical boundaries ($y=0$ and $y=-1$).

A. Boundary conditions and translated boundary conditions

Let us now determine the seven boundary conditions of the problem. We only consider the varicose mode.[4] Some conditions correspond to usual conditions for eigenmodes (homogeneous conditions at the boundaries) expressed at the porous wall, while the other ones corresponding to the chosen symmetry (varicose mode in this case) must be expressed at the symmetry line. There is no perturbation in the injection process, so that conditions at $y=-1$ are

$$\hat{u}_f=0,\quad \hat{v}_f=0,\quad \hat{u}_p=0,\quad \hat{v}_p=0,\quad \hat{\rho}_p=0. \tag{33}$$

Equations (29)–(32) show that particle and gas perturbations have the same symmetry properties, and that the varicose mode is obtained with two conditions at $y=0$:

$$\frac{d\hat{u}_f}{dy}=0,\quad \hat{v}_f=0. \tag{34}$$

Relations (33) and (34) provide the seven necessary boundary conditions for integrating (29)–(32) in the segment $[-1,0]$.

As previously noted, Eqs. (30) and (32) are not Lipschitzian at $y=0$. The solution we choose in order to circumvent this difficulty consists in translating conditions (34) from $y=0$ to $y=y_c$, where y_c is negative and close to $y=0$. This method is also employed in the axisymmetric case in order to prevent any problem near the axis.[17] Each quantity (mean flow and perturbation) is developed into a regular Taylor expansion in the vicinity of $y=0$. At leading order, with the supplementary condition $(\partial\rho_p/\partial y)(x,0)=0$, the two following relations, called translated boundary conditions (TBC), are readily obtained:

$$iy_c\alpha\check{u}_f+\check{v}_f=0,$$
$$-i\alpha Ry_c\check{p}-(-i\omega R+F_1R+i\alpha RxF_1+\alpha^2)y_c\check{u}_f \tag{35}$$
$$+\frac{d\check{u}_f}{dy}=0,$$

and these relations replace conditions (34). [Theoretically, we are sure that $(\partial\rho_p/\partial y)(x,0)$ is equal to zero if there is no injection of particles on a segment $[0,x_1]$ with $x_1>0$. But numerically, the weaker assumption $(d\tilde{\rho}_{p,w}/dx)(0)=0$ is sufficient. All the results will be presented by using it.] Notation $\check{q}$ indicates the value of the quantity $\hat{q}$ at $y=y_c$.

Finally, the stability problem to be solved reduces to Eqs. (29)–(32) with conditions (33) and (35), and the integration is done from the wall $y=-1$ up to $y=y_c$.

TABLE I. Comparison of Isakov results (on the left-hand side) and present study results (on the right-hand side) for particle-laden Poiseuille flow. The uniform mass concentration is $\rho_p=0.1$. $S_v=S/R$ is the Stokes number based on the viscous characteristic time.

S_v	R_c^{Isakov}	α_c^{Isakov}	ω_c^{Isakov}	R_c	α_c	ω_c
2×10^{-5}	6 321.2	0.9852	0.248 44	6 321.2	0.985 2	0.248 44
10^{-4}	33 340.5	0.7830	0.128 98	33 342.4	0.782 97	0.128 98
10^{-2}	6 768.3	1.0012	0.254 80	6 771.8	1.001 2	0.254 80

B. Numerical aspect

With the purpose of discretizing the eigenvalue problem, a fourth-order compact numerical scheme developed by Malik *et al.*[18] is used. The eigenvalue may be determined either by a shooting method—based on a Newton–Raphson convergence procedure—or by a LAPACK routine determining all the mathematical eigenvalues of the discretized problem. The code has been validated for the particle loaded plane Poiseuille flow, whose numerical results have been published by Isakov *et al.*[13] Table I compares the critical values, corresponding to a growth rate equal to zero, R_c, α_c, and ω_c for different Stokes numbers $S_v=S/R$ and for a uniform mass concentration $\rho_p=0.1$, which is an acceptable solution in the case of the particle-laden plane Poiseuille flow. [Because the viscous diffusion has the main role in plane Poiseuille flow stability, the Stokes number $S_v=\frac{2}{9}(a/L)^2(\rho_p^o/\rho_f)$ used by Saffman and Isakov is defined by the relaxation time versus the characteristic diffusive time. In our case, the principal actor is the convective term—*via* streamline curvature—so S corresponds to the relaxation time versus the characteristic convective time.] The code also has been validated by comparing the results to the ones for the plane monophasic Taylor flow (see Ref. 2).

C. Spectrum for temporal analysis

The discretized operator spectra in $\omega=\omega_r+\omega_i i$ (a temporal theory is used, a positive value of ω_i corresponds to an unstable basic flow) is sought by fixing α to the most spatially amplified monophasic mode obtained with ω a real number. Thus if one of the eigenvalues of the spectrum has a positive imaginary part, the particles have a destabilizing effect. Conversely, if $\omega_i<0$ the particles tend to stabilize the flow. In Figs. 4 and 5 the evolution of the eigenvalues when adding particles are plotted, for values of $(S,R,V_{p,w})$, respectively, equal to $(10^{-1}, 1000, 0.1)$ and $(10^{-3}, 1000, 1)$ and for several values of $\rho_{p,w}$ with $\alpha=3.650-0.3906i$, $x=10$, and $x_0=1$, the evolution of the eigenvalues when adding particles are plotted. In Fig. 4, the temporal growth rate ω_i decreases with $\rho_{p,w}$, so the addition of particles stabilizes the flow. On the other hand, in Fig. 5, ω_i increases with $\rho_{p,w}$; this means that the particles destabilize the flow.

Only a part of the modes which seem to exist in the single-phase flow have been plotted. Many other modes are generated by the numerical method, they do not converge when refining the grid. It has been checked, at least for monophasic modes, that the plotted ones are independent of the numerical mesh. As a conclusion, we can note that in all cases, the most amplified gas mode remains the most amplified two-phase flow mode. We did not find any counter-

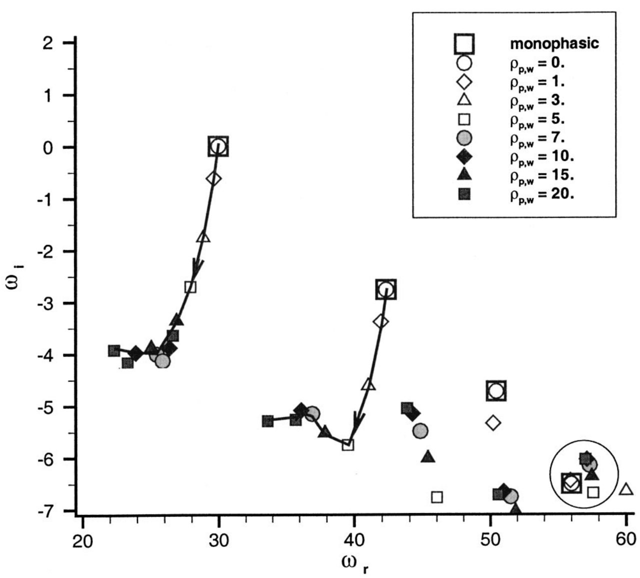

FIG. 4. Temporal spectrum. $R=1000$, $V_{p,w}=0.1$, $S=10^{-1}$. Stabilizing effect of the particles. $\alpha=3.650-0.3906i$, $x=10$, and $x_0=1$. The lines with arrows indicate a possible evolution of the single-phase eigenmodes with addition of particles. The circle points out a possible destabilization of an eigenmode but it still is stable.

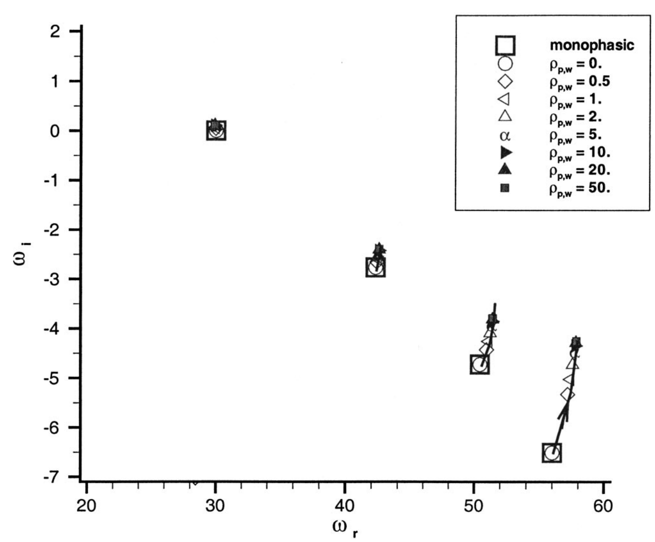

FIG. 5. Temporal spectrum. $R=1000$, $V_{p,w}=1.0$, $S=10^{-3}$. Destabilizing effect of the particles. $\alpha=3.650-0.3906i$, $x=10$, and $x_0=1$. The lines with arrows indicate a possible evolution of the single-phase eigenmodes with addition of particles.

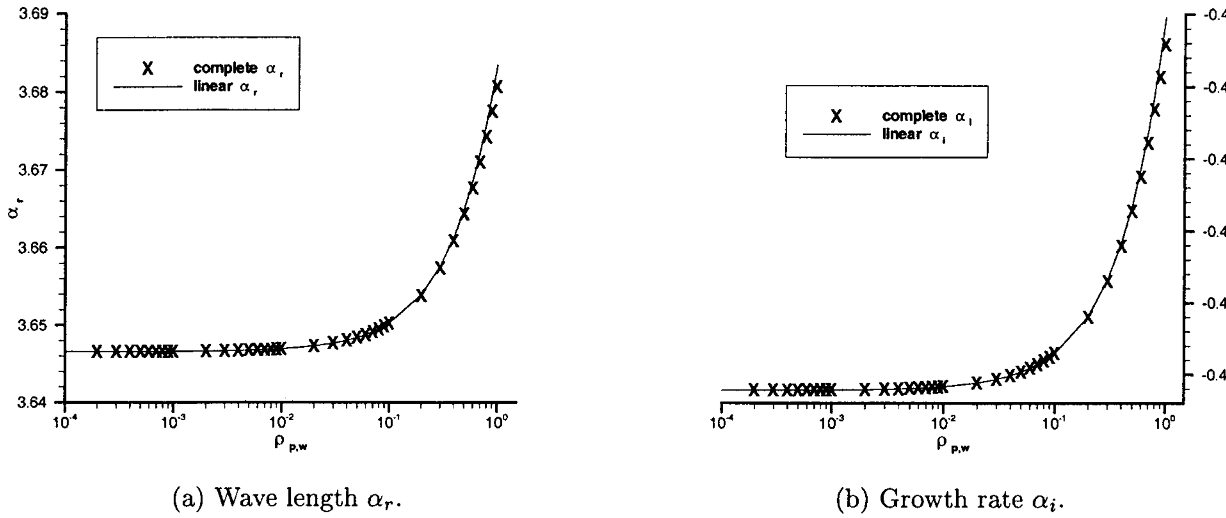

FIG. 6. Comparison of linear (solid line) and complete computations (points) in the case of weak particle mass concentrations. $V_{p,w}=0.1$, $R=10^4$, and $S=10^{-2}$.

example of such an assertion. So, we shall only study the most amplified gas mode from now on.

In Figs. 4 and 5, the square symbols represent eigenvalues obtained for the one-phase flow stability equations. It appears that particle addition in Taylor flow does not create another instability mode and only modifies monophasic instability modes. A similar proposition was given by Saffman[12] for particle laden plane Poiseuille flow.

D. Weak particle mass concentration

As explained previously, the spectra obtained either for the strictly monophasic equations or for two-phase flow equations with $\rho_{p,w}=0$ are identical. Thus, the continuity of the eigenvalues with respect to $\rho_{p,w}$ may be guessed; the goal of the present section is to demonstrate it. In this section, as in the following, results are given with the spatial linear stability theory, so only α is a complex number. As a matter of interest, if α_i is negative (the growth rate is $-\alpha_i$), the solution is unstable.

We focus the stability analysis on small values of $\rho_{p,w}$. For example, the wave number α is expanded into the form: $\alpha=\alpha_0+\rho_{p,w}\alpha_1$. Consequently, the initial eigenvalue problem $\mathcal{L}(\alpha,\rho_{p,w}).\mathcal{Z}=0$, where $\mathcal{L}(\alpha,\rho_{p,w})$ is the linear operator and $\mathcal{Z}$ the unknown vector, is written:

$$\mathcal{L}(\alpha,\rho_{p,w}).\mathcal{Z}=\mathcal{L}(\alpha_0,0).\mathcal{Z}_0+\rho_{p,w}\left(\alpha_1\frac{\partial\mathcal{L}}{\partial\alpha}(\alpha_0,0).\mathcal{Z}_0+\frac{\partial\mathcal{L}}{\partial\rho_{p,w}}(\alpha_0,0).\mathcal{Z}_0+\mathcal{L}(\alpha_0,0).\mathcal{Z}_1\right)+o(\rho_{p,w}).$$

At order 0, the known monophasic problem is recovered:

$$\mathcal{L}(\alpha_0,0).\mathcal{Z}_0=0. \tag{36}$$

At order 1, an inhomogeneous problem is obtained:

$$\mathcal{L}(\alpha_0,0).\mathcal{Z}_1=-\alpha_1\frac{\partial\mathcal{L}}{\partial\alpha}(\alpha_0,0).\mathcal{Z}_0-\frac{\partial\mathcal{L}}{\partial\rho_{p,w}}(\alpha_0,0).\mathcal{Z}_0=-\mathcal{L}^1.\mathcal{Z}_0, \tag{37}$$

where α_1 and $\mathcal{Z}_1$ are the unknown parameters. With the purpose of determining the correction α_1 of the complex wave number α, the Fredholm alternative is used. It shows that the algebra-type problem $\mathcal{A}\cdot u=f$, where $\mathcal{A}$ is not invertible may have solutions only if the given function f is orthogonal to the kernel of the adjoint operator $\mathcal{A}^*$. In our case, the operator $\mathcal{L}(\alpha_0,0)$ is not invertible because α_0 is searched as an eigenvalue of it, so $(-\mathcal{L}^1.\mathcal{Z}_0)$ must verify the orthogonality condition

$$(\mathcal{Z}^*|-\mathcal{L}^1.\mathcal{Z}_0)=0, \tag{38}$$

where $\mathcal{Z}^*$ belongs to the kernel of the adjoint operator $\mathcal{L}_0^*$ of $\mathcal{L}(\alpha_0,0)$. Relation (38), called "solvability condition" gives the linear correction α_1.[19]

In order to determine the latter, the first task consists in solving the adjoint problem. Keeping in mind that the direct problem $\mathcal{L}(\alpha_0,0)$ is not Lipschitzian at $y=0$, so the adjoint $\mathcal{L}_0^*$ is. Therefore, as has been done for the direct problem, TBC must be determined at y_c for the adjoint operator. Two techniques are possible.

(1) The adjoint operator is calculated in the segment $[-1,0]$, so boundary conditions at $y=0$ are determined directly. The same procedure used for the direct problem is applied. This gives a set of conditions at $y=y_c$ to solve $\mathcal{L}_0^*$.
(2) The adjoint operator is determined in $[-1,y_c]$ and TBC for $\mathcal{L}_0^*$ are determined in order to eliminate the nonintegral terms which appear in the integration by part used for the calculation of the adjoint operator.

For TBC of order $n=1$, the two ways lead exactly to the same analytical expressions presented in Appendix B.

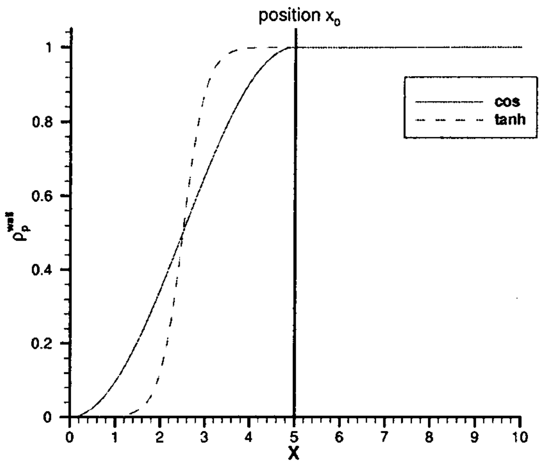

(a) Two shapes: cos and tanh

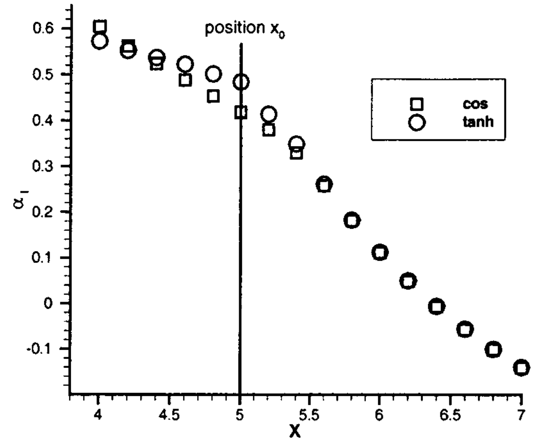

(b) Imaginary part α_i.

FIG. 7. Influence of the boundary condition shape on stability results. Evolution of the imaginary part α_i of the eigenvalue α vs $\rho_{p,w}$ for two kinds of parietal particle concentration law $\tilde{\rho}_{p,w}(x)$ plotted on the left-hand side with $x_0=5$. $V_{p,w}=1$, $R=10^3$, $S=10^{-3}$, and $\rho_{p,w}=1$. Abscissa x varying from 4 to 7.

Results from the linearized behavior with the mass concentration at the propellant surface $\rho_{p,w}$ (solid line) and from the complete computation (points) are presented in Fig. 6, for a Stokes number $S=10^{-2}$, a Reynolds number $R=10^4$, and a particle speed ejection $V_{p,w}=0.1$. Both methods give comparable results for parietal mass density $\rho_{p,w}$ up to 0.1 ($\rho_{p,w}.V_{p,w}=10^{-2}$); this is true for the wavelength α_r (on the left) and the growth rate α_i (on the right).

E. Parametric study

In this section, results from various computations are shown in order to give some ideas on the influence of each parameter on stability characteristics. We successively look at the influence of the shape of $\tilde{\rho}_{p,w}$, the x_0 value (upstream abscissa of the constant particle mass concentration at the porous wall), the value of $V_{p,w}$, and large values of $\rho_{p,w}$.

1. Influence of the shape of $\tilde{\rho}_{p,w}$ and of x_0

To solve the PDE (26) in order to determine ρ_p, the boundary condition at $y=-1$, $\tilde{\rho}_{p,w}$ must be specified. Its value and its first derivative at $x=0$ are set equal to 0 and a nonzero constant value $\rho_{p,w}$ is imposed for $x\geqslant x_0$. But the shape of $\tilde{\rho}_{p,w}$ for $0<x<x_0$ is not known, it is an artifact allowing ρ_p to be bounded close to the symmetry line. Then it cannot have any influence on stability results. Two different shapes have been tested called "cos" and "tanh" whose expressions are, respectively,

$$\text{``cos''}\quad \begin{cases} \rho_{p,w} & \text{if } x>x_0 \\ \rho_{p,w}\dfrac{1-\cos\big(\pi(x/x_0)\big)}{2} & \text{if } x<x_0, \end{cases}$$

$$\text{``tanh''}\quad \rho_{p,w}\frac{\tanh(10(x/x_0)-5)+\tanh 5}{2\tanh 5}.$$

The left-hand side of Fig. 7 gives two different shapes of the function $\tilde{\rho}_{p,w}$ with $x_0=5$ with the corresponding stability results (growth rate) plotted on the right-hand side. As can be observed, results are rapidly brought together downstream of the position x_0, so that the shape of the boundary condition does not have any influence on stability results. This can be explained by the following remark. The injected mass defect is convected by the gas so that for large x/x_0 values this defect is rejected close to $y=0$, and we know that the instability is mainly governed by the streamline curvature near the porous wall.[4] In the following, x_0 is fixed to 1. As the basic single-phase flow becomes unstable from $x\approx 5$, the influence of the shape of the injection for $x\leqslant x_0$ is negligible in the amplified regime.

TABLE II. Influence of particle ejection speed $V_{p,w}$ on correction α_1 at $x=10$ with $x_0=1$ and $\omega=30$.

R	S	$V_{p,w}$	$\frac{P_\rho(V_{p,w})}{P_\rho(V_{p,w}=1)}$	$\mathrm{Re}(\alpha_1)$	$\mathrm{Im}(\alpha_1)$	$\frac{\mathrm{Re}(\alpha_1)(V_{p,w})}{\mathrm{Re}(\alpha_1)(V_{p,w}=1)}$	$\frac{\mathrm{Im}(\alpha_1)(V_{p,w})}{\mathrm{Im}(\alpha_1)(V_{p,w}=1)}$
10^3	10^{-3}	1.0	1.0	3.3023×10^{-2}	-3.1627×10^{-2}	1.0	1.0
10^3	10^{-3}	10^{-1}	9.88×10^{-2}	3.3503×10^{-3}	-3.1129×10^{-3}	1.01×10^{-1}	9.84×10^{-2}
10^3	10^{-3}	10^{-2}	1.12×10^{-2}	3.8244×10^{-4}	-3.5520×10^{-4}	1.15×10^{-2}	1.12×10^{-2}
10^4	10^{-1}	1.0	1.0	0.807 69	1.034 6	1.0	1.0
10^4	10^{-1}	10^{-1}	9.93×10^{-2}	$7.822\,2\times10^{-2}$	0.138 91	9.68×10^{-2}	1.34×10^{-1}
10^4	10^{-1}	10^{-2}	9.84×10^{-3}	$7.723\,8\times10^{-3}$	$1.380\,3\times10^{-2}$	9.56×10^{-3}	1.33×10^{-2}
10^4	10^{-1}	10^{-3}	1.12×10^{-3}	$8.829\,1\times10^{-4}$	$1.577\,9\times10^{-3}$	1.09×10^{-3}	1.52×10^{-3}

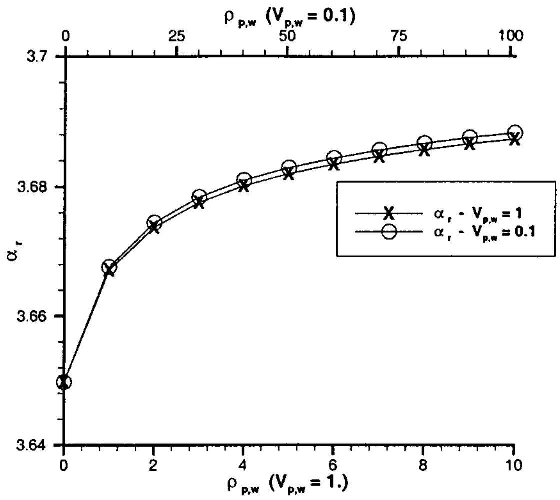

(a) Wave number α_r.

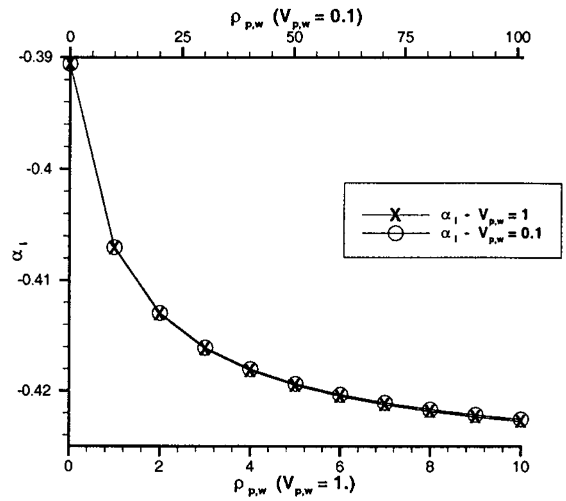

(b) Imaginary part α_i.

FIG. 8. Dependency of number α with particle mass concentration ratio $P_\rho(V_{p,w})/P_\rho(V_{p,w}=1)$ created by two different ejection speeds $V_{p,w}=1$ and $V_{p,w}=0.1$: $P_\rho(V_{p,w}=0.1)/P_\rho(V_{p,w}=1)\simeq 9.89\times 10^{-2}$. $R=10^3$, $S=10^{-3}$. $x=10$ and $x_0=1$.

2. Influence of $V_{p,w}$

Now, let us have a look at the role of injection speed of the particles $V_{p,w}$ on stability results. In Fig. 8, the values of the real and imaginary parts of α are plotted as function of $\rho_{p,w}$ for two values of $V_{p,w}$. The two x abscissas are scaled together in order to have $\rho_{p,w}(V_{p,w}=1)=K.\rho_{p,w}(V_{p,w}=0.1)$ with K being the ratio of the two plateau values (9.89×10^{-2} as indicated in the caption). The plateau P_ρ has been defined in Sec. IV D, see also Fig. 3. For α_r and for α_i, the two curves are superimposed, the values of α are consequently determined by the plateau for each particle injection velocity:

$$\alpha(V_{p,w},\rho_{p,w})\simeq\alpha\left(V_{p,w}=1,\frac{P_\rho(V_{p,w})}{P_\rho(V_{p,w}=1)}\rho_{p,w}\right). \tag{39}$$

This simple expression is confirmed in Table II obtained for weak values of $\rho_{p,w}$ as described in Sec. V D. In that case the previous relationship (39) becomes

$$\alpha_1(V_{p,w})\simeq\frac{P_\rho(V_{p,w})}{P_\rho}\alpha_1(V_{p,w}=1). \tag{40}$$

As indicated in Table II, this estimation works better for weak Stokes numbers.

Relation (40) points out the role of the plateau P_ρ. It is interesting to note that this value P_ρ may be estimated for small Stokes numbers. In this case, very close to the wall, the particle transverse velocity evolves rapidly from $V_{p,w}$ to $V_{f,w}$ ($=1$), whereas the particle longitudinal velocity is negligible, so that the control volume, with a fixed number of particles, is divided by $V_{p,w}$. Consequently, the concentration ρ_p evolves rapidly from $\rho_{p,w}$ to the plateau $P_\rho=\rho_{p,w}V_{p,w}$. Finally the correction α_1 is proportional to $V_{p,w}$ (in particular the sign of α_1 is not modified by $V_{p,w}$).

3. Case of large values of $\rho_{p,w}$

Figures 9 and 10 show that by increasing $\rho_{p,w}$, instability wave numbers get closer to inviscid flow instability ones. In order to understand such behavior, it must be pointed out that increasing particle mass concentration is like increasing the mass density ρ_f of the fluid for the definition of the Reynolds number. In fact, for $\rho_{p,w}\gg 1$, perturbed fluid momentum equations (31) indicates $\hat{u}_{f,i}\sim\hat{u}_{p,i}$, so that (31) and (32) lead to $[(41)\leftarrow(31)-\overline{\rho_p}\times(32)]$:

$$\begin{aligned}
&-i\omega\hat{u}(1+\overline{\rho_p})+\hat{u}(F'+\overline{\rho_p}G)+\hat{v}x(F''+\overline{\rho_p}G')\\
&\quad+i\alpha x\hat{u}(F'+\overline{\rho_p}G)+(\overline{\rho_p}J-F)\frac{d\hat{u}}{dy}\\
&\quad=-i\alpha\hat{p}+\frac{1}{R}\left(\frac{d^2\hat{u}}{dy^2}-\alpha^2\hat{u}\right)+\frac{\hat{\rho}_p}{S}x(G-F')\\
&\qquad+O\left(\hat{u},\hat{v},\frac{d\hat{u}}{dy},\hat{p}\right),\\
&-i\omega\hat{v}(1+\overline{\rho_p})-\hat{v}(F'+\overline{\rho_p}G)+i\alpha x\hat{v}(F'+\overline{\rho_p}G)\\
&\quad+(\overline{\rho_p}J-F)\frac{d\hat{v}}{dy}\\
&\quad=-\frac{d\hat{p}}{dy}+\frac{1}{R}\left(\frac{d^2\hat{v}}{dy^2}-\alpha^2\hat{v}\right)\\
&\qquad+\frac{\hat{\rho}_p}{S}(J+F)+O\left(\hat{u},\hat{v},\frac{d\hat{u}}{dy},\hat{p}\right).
\end{aligned} \tag{41}$$

The left-hand-side terms of Eq. (41) are of order

$$\begin{aligned}
&\mathcal{O}_{\mathrm{conv}}=\min(\|(1+\overline{\rho_p})\|_2,\|(F'+\overline{\rho_p}G)\|_2,\\
&\quad\|(F''+\overline{\rho_p}G')\|_2,\|(\overline{\rho_p}J-F)\|_2)\simeq(1+P_\rho),
\end{aligned}$$

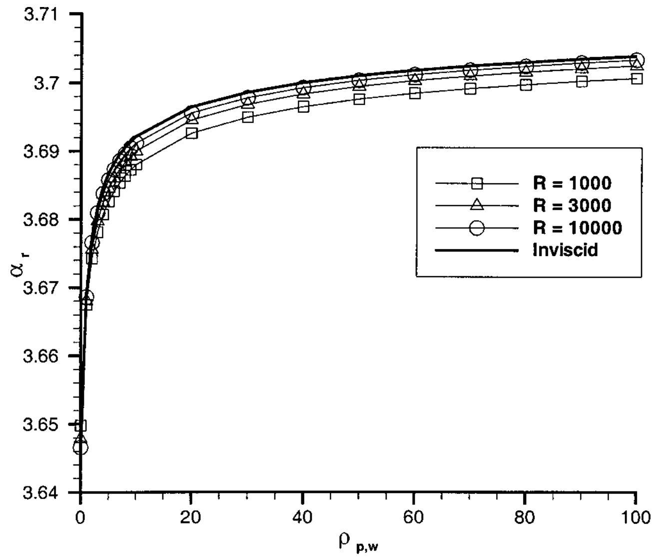

FIG. 9. Evolution of the wave number α_r with mass concentration at the propellant surface. $S=10^{-3}$, $V_{p,w}=1$, $\omega=30$, $x=10$, and $x_0=1$. Pinching of the viscous results toward inviscid results.

so that the characteristic value of the convective term $\mathcal{O}_{\text{conv}}$ is not only larger than the characteristic value of the diffusive term of order $1/R$, but is increasing with $\rho_{p,w}$. Therefore the effective Reynolds number is much larger, for $\rho_{p,w}\gg 1$, than the one used by definition. Care must be taken in defining $\mathcal{O}_{\text{conv}}$ which is estimated by the quadratic norm $\|X\|_2$, which corresponds to the quadratic average of the function X in $[-1,y_c]$. But, $\rho_p(x,0)=0$ and $(\partial\rho_p/\partial y)(x,0)=0$, so that in a neighborhood of the axis $y=0$, convective and diffusive terms are of the same order as in the single-phase flow. This may explain the small but persistent differences observed for large particle mass concentration level $\rho_{p,w}$ between viscous and inviscid results. If the convergence is not proved, the

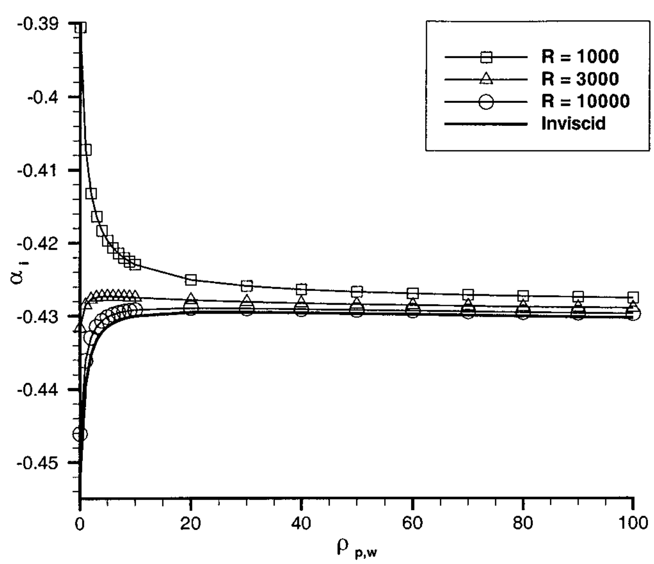

FIG. 10. Evolution of the growth rate $-\alpha_i$ with mass concentration at the propellant surface. $S=10^{-3}$, $V_{p,w}=1$, $\omega=30$, $x=10$, and $x_0=1$. Pinching of the viscous results toward inviscid results.

pinching of stability results for both viscous and inviscid flow is. As only the viscous Stokes drag term is kept and only a one-way coupling computation is done, the present analysis is actually limited to small particle mass concentration. However, the previous remark gives a practical tool for determining the main tendencies: knowledge of the monophasic growth rate and of the inviscid evolution of α with respect to $\rho_{p,w}$ (at the prescribed S value) determines whether particles stabilize the flow or not, at least at large particle mass concentration. If the monophasic growth rate value at fixed Reynolds number R is larger than the inviscid growth rate values for large value of $\rho_{p,w}$, then particles stabilize the flow. Conversely, particles destabilize the flow when monophasic growth rate value is lower than the inviscid growth rate value obtained for large $\rho_{p,w}$. Thanks to the monotonous evolution of α with respect to $\rho_{p,w}$ (at least when the monophasic wave number is not close to the limit value of α given by the inviscid result), the last remark may constitute a criterion for the determination of the effect of the addition of particles upon stability. The sign of the modified growth rate also provides a similar criterion but only for small particle concentrations.

VI. CONCLUSION

The present study is a first investigation of the particle effect upon Taylor flow stability, whose knowledge is relevant in order to understand thrust oscillations of solid-propellant motors. First, a solution in a self-similar form is found for both fluid and particle velocity fields when the condition $4SF'(0)\leq 1$ is fulfilled. The particle mass concentration ρ_p cannot be sought in a self-similar form because of its divergence near the symmetry line $y=0$, so that a PDE has to be solved in the (x, y) plane. A linear stability study is performed for this particular flow. Based on the spectrum of the linearized problem, it appears that particles would not create extra instability modes compared with the single-phase flow, but would only modify its modes. The study of tiny particle mass concentration enables us to determine a linear correction of α from the monophasic study, and to demonstrate the expected continuity of stability parameters from one-phase to two-phase flow. Finally, it appears that particles act upon the Reynolds number R by virtually reducing fluid viscosity or increasing the mass density of the associated flow, as described by Saffman[12] and Isakov and Rudnyak.[13] It follows that the added particles tend to bring stability modes close to two-phase flow inviscid modes. The role of the ejection speed $V_{p,w}$ is also explained: it mainly exerts influence on particle mass concentration especially by changing the plateau P_ρ, whose influence on stability appears to be nearly linear. Finally, in order to know if particles stabilize or not, a simple criteria is proposed: it is based on inviscid results for large $\rho_{p,w}$ and monophasic results. Then, as the Reynolds number and the Stokes number are known, so the limit value of α is, given by inviscid results, and the rate of particle influence α_1, characterizing the convergence speed to inviscid results.

ACKNOWLEDGMENTS

The present study has been supported by the French Centre National d'Etudes Spatiales (CNES) and by the National French Establishment for Aerospace Research (ONERA).

APPENDIX A: STABILITY SYSTEM FOR THE PARTICLE LOADED TAYLOR FLOW

As noted in Sec. V, the linear operator for stability can be written in the following form:

$$\frac{d\mathcal{Z}}{dy}=D\mathcal{Z},$$

with the unknown vector $\mathcal{Z}$ on the form

$$\mathcal{Z}=\left(\hat{u}_f,\frac{d\hat{u}_f}{dy},\hat{v}_f,\hat{p},\hat{u}_p,\hat{v}_p,\hat{\rho}_p\right)^T,$$

where V^T is the transpose of vector V. Matrix D is of the form

$$D=\begin{pmatrix} 0 & 1 & 0 & 0 & 0 & 0 & 0\\ d_{2,1} & d_{2,2} & d_{2,3} & d_{2,4} & d_{2,5} & 0 & d_{2,7}\\ d_{3,1} & 0 & 0 & 0 & 0 & 0 & 0\\ d_{4,1} & d_{4,2} & d_{4,3} & 0 & 0 & d_{4,6} & d_{4,7}\\ d_{5,1} & 0 & 0 & 0 & d_{5,5} & d_{5,6} & 0\\ 0 & 0 & d_{6,3} & 0 & 0 & d_{6,6} & 0\\ 0 & 0 & d_{7,3} & 0 & d_{7,5} & d_{7,6} & d_{7,7} \end{pmatrix},$$

whose nonzero coefficients are

$$d_{2,1}=-i\omega R+R\frac{\partial U_f}{\partial x}+i\alpha RU_f+\alpha^2+\frac{R\rho_p}{S},$$

$$d_{2,2}=RV_f,$$

$$d_{2,3}=R\frac{\partial U_f}{\partial y},$$

$$d_{2,4}=i\alpha R,$$

$$d_{2,5}=-\frac{R\rho_p}{S},$$

$$d_{2,7}=\frac{R}{S}(U_f-U_p),$$

$$d_{3,1}=-i\alpha,$$

$$d_{4,1}=i\alpha V_f,$$

$$d_{4,2}=-\frac{i\alpha}{R},$$

$$d_{4,3}=i\omega-\left(\frac{\alpha^2}{R}+\frac{\rho_p}{S}+i\alpha U_f+\frac{dV_f}{dy}\right),$$

$$d_{4,6}=\frac{\rho_p}{S},$$

$$d_{4,7}=\frac{V_p-V_f}{S},$$

$$d_{5,1}=\frac{1}{SV_p},$$

$$d_{5,5}=\frac{1}{V_p}\left(-i\alpha U_p-\frac{1}{S}-\frac{\partial U_p}{\partial x}+i\omega\right),$$

$$d_{5,6}=-\frac{1}{V_p}\frac{\partial U_p}{\partial y},$$

$$d_{6,3}=\frac{1}{SV_p},$$

$$d_{6,6}=\frac{1}{V_p}\left(-i\alpha U_p-\frac{1}{S}-\frac{dV_p}{dy}+i\omega\right),$$

$$d_{7,3}=-\frac{\rho_p}{SV_p^2},$$

$$d_{7,5}=\frac{1}{V_p}\left(-i\alpha\rho_p-\frac{\partial\rho_p}{\partial x}\right),$$

$$d_{7,6}=\frac{1}{V_p}\left(-\frac{\partial\rho_p}{\partial y}+\frac{\rho_p}{V_p}\left(\frac{1}{S}+i\alpha U_p+\frac{dV_f}{dy}-i\omega\right)\right),$$

$$d_{7,7}=\frac{1}{V_p}\left(-i\alpha U_p-\frac{\partial U_p}{\partial x}-\frac{dV_p}{dy}+i\omega\right).$$

APPENDIX B: ADJOINT OPERATOR BOUNDARY CONDITIONS

In Sec. V D the Fredholm alternative is used in order to define the linear correction α_1 to the monophasic number α. As already said in Sec. V D, two possible ways for determining the TBC of the adjoint problem exist. First, TBC can be sought from knowledge of the boundary conditions at $y=0$ of the adjoint problem and the technique is the same as in the case of the direct problem: these conditions are translated from $y=0$ to $y=y_c$. The second way is that the TBC are directly obtained from the integration by parts that leads to the adjoint operator, in this case, the integration is done on the segment $[-1,y_c]$. The purpose of this appendix is to give explicitely the TBC obtained with an expansion of the first order of the eigenfunctions.

At $y=y_c$:

(1) $\mathcal{Z}_5^*=0$,
(2) $\mathcal{Z}_6^*=0$,
(3) $\mathcal{Z}_7^*=0$,

(4) $i\alpha^0R\mathcal{Z}_2^*+\mathcal{Z}_4^*/y_c=0$,
(5) $\mathcal{Z}_1^*/y_c-i\alpha^0\mathcal{Z}_3^*+(R(-i\omega+F_1+ixF_1\alpha^0)+(\alpha^0)^2)\mathcal{Z}_2^*=0$,

and at $y=-1$:

(1) $\mathcal{Z}_2^*=0$,
(2) $\mathcal{Z}_4^*=0$.

The conditions have been obtained by the two different methods.

[1] V. Varapaev and V. Yagodkin, ''Flow instability in a channel with porous walls,'' Izv. Akad. Nauk SSSR, Mekh. Zhidk. Gaza **4**, 91 (1969).
[2] G. Casalis, G. Avalon, and J.-P. Pineau, ''Spatial instability of planar channel flow with fluid injection through porous wall,'' Phys. Fluids **10**, 2558 (1998).
[3] G. Taylor, ''Fluid flow in regions bounded by porous surfaces,'' Proc. R. Soc. London, Ser. A **234**, 456 (1956).
[4] J. Griffond, ''Instabilité pariétale et accrochage aéroacoustique dans les conduits à parois débitantes simulant les moteurs à propergol solide d'Ariane 5,'' Ph.D. thesis, Supaéro, Toulouse, France, September 2001.
[5] G. Avalon and G. Casalis, ''Instabilités et prévision de l'accrochage acoustique des écoulements avec injection pariétale,'' Third Conference R&D Écoulements Internes en Propulsion Solide, Poitiers, France, 25–27 March 1998.
[6] J. Griffond, ''Receptivity and aeroacoustic resonance in channels with blowing walls,'' Phys. Fluids **14**, 3946 (2002).
[7] J. Majdalani and T.-S. Roh, ''The oscillatory channel flow with large wall injection,'' Proc. R. Soc. London, Ser. A **456**, 1625 (2000).
[8] G. Flandro, ''Effects of vorticity on rocket combustion stability,'' J. Propul. Power **11**, 607 (2000).
[9] J. Dupays, ''Contribution à l'étude du rôle de la phase condensée dans la stabilité d'un propulseur à propergol solide pour lanceur spatial,'' Tech. Report, ONERA technical note, June 1997.
[10] N. Lupoglazoff, F. Vuillot, J. Dupays, and Y. Fabignon, ''Numerical simulations of the unsteady flow inside Ariane 5 P230 SRM booster with burning aluminium particles,'' Second European Conference on Launcher Technology Solid Space Propulsion, Roma, Italy, 21–24 November 2000.
[11] E. Daniel and N. Thévand, ''Stability of acoustic wave in two-phase dilute flow with mass transfer,'' AIAA J. **39**, 2121 (2001).
[12] P. Saffman, ''On the stability of laminar flow of a dusty gas,'' J. Fluid Mech. **13**, 120 (1962).
[13] E. Isakov and V. Rudnyak, ''Stability of rarefied dusty gas and suspension flows in a plane channel,'' Fluid Dyn. **30** (5) (1995).
[14] T. Féraille, G. Casalis, and J. Dupays, ''Particle effects on solid-propellant motors flow stability,'' AIAA-2002-3611, 38th AIAA/ASME/SAE/ASEE Joint Propulsion Conference & Exhibit, Indianapolis, IN, 7–10 July 2002.
[15] A. S. Berman, ''Laminar flow in channels with porous walls,'' J. Appl. Phys. **24**, 1232 (1953).
[16] J. Griffond and G. Casalis, ''On the nonparallel stability of the injection induced two-dimensional Taylor flow,'' Phys. Fluids **13**, 1635 (2000).
[17] J. Griffond, G. Casalis, and J. Pineau, ''Spatial instability of flow in a semiinfinite cylinder with fluid injection through its porous walls,'' Eur. J. Mech. B/Fluids **19**, 69 (2000).
[18] M. Malik, S. Chuang, and M. Hussaini, ''Accurate numerical solution of compressible, linear stability equations,'' J. Appl. Math. Phys. **33**, 189 (1982).
[19] A. Nayfeh, *Introduction to Perturbation Techniques*, Classics Library ed. (Wiley, New York, 1993).